Editors' Suggestion | Featured in Physics

Laser Probing of the Rotational Cooling of Molecular Ions by Electron Collisions

Ábel Kálosi,[1,2,*] Manfred Grieser,[1] Robert von Hahn,[1] Ulrich Hechtfischer,[1,†] Claude Krantz,[1,‡] Holger Kreckel,[1] Damian Müll,[1] Daniel Paul,[1,2] Daniel W. Savin,[2] Patrick Wilhelm,[1] Andreas Wolf,[1] and Oldřich Novotný[1]

[1]*Max-Planck-Institut für Kernphysik, Saupfercheckweg 1, D-69117 Heidelberg, Germany*

[2]*Columbia Astrophysics Laboratory, Columbia University, New York, New York 10027, USA*

(Received 17 August 2021; revised 2 March 2022; accepted 23 March 2022; published 4 May 2022)

We present state-selected measurements of rotational cooling and excitation rates of CH^+ molecular ions by inelastic electron collisions. The experiments are carried out at a cryogenic storage ring, making use of a monoenergetic electron beam at matched velocity in combination with state-sensitive laser dissociation of the CH^+ ions for simultaneous monitoring of the rotational level populations. Employing storage times of up to 600 s, we create conditions where electron-induced cooling to the $J = 0$ ground state dominates over radiative relaxation, allowing for the experimental determination of inelastic electron collision rates to benchmark state-of-the-art theoretical calculations. On a broader scale, our experiments pave the way to probe inelastic electron collisions for a variety of molecular ions relevant in various plasma environments.

DOI: 10.1103/PhysRevLett.128.183402

Electron collisions with molecular ions are fundamental processes in partially ionized molecular gas, ranging from astrophysical environments and planetary atmospheres to low temperature plasma used in advanced technologies [1,2]. Despite their fundamental relevance, detailed experimental data on the effect of electron collisions on the internal excitation of the molecular ions are essentially nonexistent. Moreover, to enable computationally tractable calculations, most state-of-the-art theoretical methods require significant approximations [3], such as the Coulomb-Born (CB) [4–7] and R-matrix methods [8–15], which in this context have remained without experimental verification. For rotationally inelastic collisions between electrons and molecular ions, in particular, theoretical calculations have not yet converged [4–13,16–18], and we are unaware of any previous state-resolved experimental cross section data that can guide the theory.

For illustration, we consider the case of molecular ions in cold astrophysical environments [19,20]. They are mostly observed [21] by radio-astronomy via transitions between the lowest rotational states, requiring knowledge of the inelastic collision processes that contribute to rotational excitation and de-excitation. At the relevant temperatures of 10–100 K, the dominant partners for inelastic collisions are hydrogen atoms or molecules, and electrons [13,18]. Electronic collisions are relevant even at the generally small electron density in the interstellar medium (typically $\sim 10^{-4}$ of hydrogen) because of their higher rate coefficients (10^{-6} cm^3 s^{-1} at 10–100 K for dipolar molecular ions). For ions such as HCO^+, electron collisions are found to even dominate the inelastic rates [18].

To represent, in particular, the astrophysical conditions, relevant laboratory studies should ensure the low-density, binary-collision regime. Hence, very sensitive detection methods are required. Moreover, the internal molecular excitation must be probed for only a few populated rotational levels, corresponding to the cold astrophysical temperatures. We present such a measurement using methylidyne (CH^+) cations circulating in a cryogenic storage ring. There, the rotational level populations are subject to radiative cooling in the cryogenic environment and to controlled electron collisions in a merged, velocity-matched beam of electrons. We probe the evolution of the level populations as a function of storage time by resonant photodissociation. At effective temperatures of ~20 K for the radiation field and ~26 K for the electrons, we reach effective electron densities substantially above the critical density needed for collisional transition rates to dominate over the radiative ones. Hence, rotational cooling by inelastic electron collisions outperforms radiative cooling, leading to $J = 0$ as the dominant rotational level after a much shorter storage time than for radiative cooling alone. Using laser diagnostics, the electron-induced changes of the rotational populations are measured and compared to theory. This confirms recent predictions for the low-temperature inelastic rate coefficients of CH^+ and demonstrates that, in combination with suitable rotational diagnostics, cryogenic storage rings offer a platform to measure rotationally inelastic electron-collision rates for a wide range of molecular ions.

Merged-beams studies in room-temperature storage rings [22] demonstrated the effect of electron collisions on rotational excitation of HD^+ by measuring the fragmentation energies from dissociative recombination (DR) events. However, individual angular momenta J could not be resolved, and the effect of electron collisions on the rotational populations was far from dominant. Cryogenic storage rings for molecular ions [23,24] now enable state-selective studies for the lowest J levels of elementary diatomic ions. These studies addressed spontaneous radiative relaxation of rotational excitation in a low-temperature blackbody field for CH^+ [25] and OH^- [26,27]. Moreover, the rotational dependence of the low-energy DR rate was measured in electron collision experiments on HeH^+ [28]. The present Letter extends these studies by combining laser probing of the rotational level populations of CH^+ ions with the collisional rotational cooling of these ions by a merged electron beam.

The experiments are performed in the cryogenic storage ring (CSR) [24] at the Max Planck Institute for Nuclear Physics in Heidelberg, Germany. A 280-keV beam of CH^+ ions with a broad J distribution is produced in a Penning ion source, electrostatically accelerated, and injected into the CSR, where the ions then circulate with a mean storage lifetime of ~180 s. For rotational diagnostics, they are illuminated in a straight section of the ring with nanosecond laser pulses from an optical parametric oscillator (OPO) with a tunable wavelength near 300 nm. At certain wavelengths, CH^+ ions in specific low-J levels can be preferentially addressed by resonant photodissociation, as already demonstrated at CSR [25]. Neutral H atoms from the photodissociation leave the closed ion orbit at a downstream electrostatic deflector and are counted on a microchannel plate (MCP) detector [Fig. 1(a)].

On each revolution, the ions interact with the velocity-matched, collinear electron beam of the CSR electron cooler. The electron cooler delivers a continuous, nearly monoenergetic electron beam of ~20 eV, guided by an axial magnetic field (10 mT in the interaction region) to yield a 10-mm diameter, nearly homogeneous current density profile in the collinear overlap region with the ion beam. The electron density is $7.0(6) \times 10^5$ cm^{-3} (here and below, the number in parentheses is the one-sigma uncertainty of the final digit), and the relative velocities are mainly transverse to the beam direction with an effective temperature $T_\perp \sim 26$ K [$k_B T_\perp = 2.25(25)$ meV with k_B being the Boltzmann constant; further discussed below]. The overlap region is housed in a biased drift tube where the electrons are decelerated to 11.8 eV, thus reaching the same velocity as the stored CH^+ ions over an effective matched-velocity overlap region of 0.79(1) m. The ion beam is centered within the electron beam and reaches an effective full width at half-maximum (FWHM) diameter of < 6 mm after 10 s of phase-space cooling by the electrons [29]. The DR rate and its dependence on the electron-ion collision energy are measured using the MCP detector. The peak in the DR rate at the lowest achievable electron-ion collision energy serves for matching the average ion and electron beam velocities.

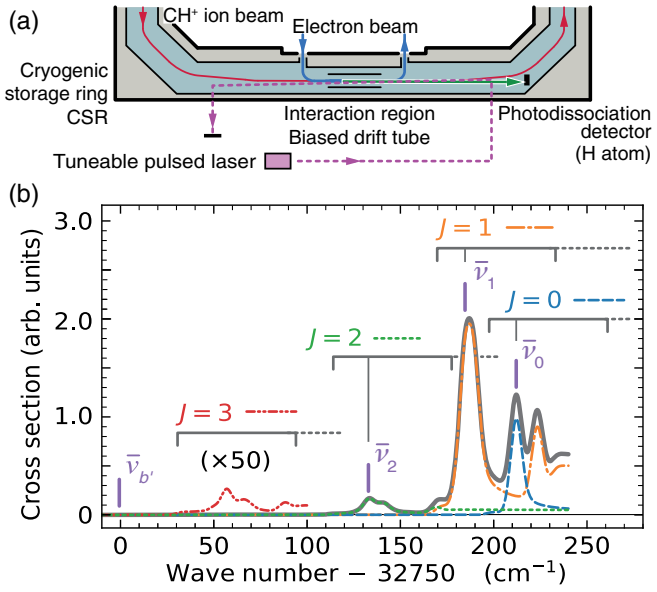

FIG. 1. (a) Schematic of the storage-ring section for laser probing and merged-beam electron-ion interaction. (b) Theoretical near-threshold photodissociation cross sections of CH^+ ions [25] in $J \leq 3$, weighted with a typical J distribution during rotational relaxation in the CSR and convolved with the laser line shape (FWHM 6.1 cm^{-1}). Horizontal brackets: wave number ranges between the thresholds for $C^+(^2P_{1/2})$, lower, and $C^+(^2P_{3/2})$, upper, for the indicated J. Thick vertical lines mark the wave numbers $\bar{\nu}_i$ ($i = 0, \ldots, 2$) and $\bar{\nu}_{b'}$ where laser probing signals were accumulated. The probing wave numbers are Doppler shift corrected, as explained in the Supplemental Material [29]. Individual J contributions (broken curves) add up to the total probed signal (full curve). The magnified contribution of $J = 3$ is shown up to the onset of its continuum level only.

CH^+ [29] has an $X^1\Sigma^+$ ground state with a rotational constant of ~13.9 cm^{-1} and a dissociation energy $D_0 = 32946.7(11)$ cm^{-1} [30]. A metastable $a^3\Pi$ state with ~1.2 eV excitation energy and measured lifetime of ~7 s [37] is strongly populated in the injected ion beam [29]. At a storage time $t \gtrsim 20$ s, radiative relaxation has progressed along the vibrational cascades (all having radiative lifetimes $\tau_r < 0.1$ s) while the rotational cascade then has essentially depopulated the $J \geq 4$ states [$\tau_r < 2$ s for $X^1\Sigma^+(v = 0)$]. The population in the metastable $a^3\Pi$ levels was monitored *in situ* by storage-time-dependent molecular-fragment imaging making use of the unique signature of DR from these levels. Their fractional populations were found to be < 0.1 for $t > 25$ s and < 0.05 for $t > 40$ s [29]. For $t > 20$ s, we probe the populations of the remaining levels, $X^1\Sigma^+(v = 0, J \leq 3)$, via Feshbach resonances in near-threshold photodissociation [25,30,49].

In this process, optical transitions excite the $A^1\Pi$ electronic state which correlates to the atomic channel $H + C^+(^2P_{3/2})$ with a fine-structure excitation of 63.42 cm^{-1} [50] and supports vibrational energy levels above the $H + C^+(^2P_{1/2})$ channel. These levels dissociate by spin-orbit and rotational coupling while being long-lived enough to cause distinct resonances [30] in the near-threshold photodissociation spectrum.

Considering the initial $CH^+(X^1\Sigma^+, v = 0, J)$ levels, the photodissociation yield as a function of the photon energy has characteristic resonances for each J [Fig. 1(b)]. In our laser-probing scheme, we use three photon wave numbers $\bar{\nu}_i$ controlled by the OPO laser tuning, each situated near a J resonance peak for $J \leq 2$. Gated count rates R_i were accumulated in time windows synchronized with the arrival times of H atoms produced by the < 10-ns laser pulses (repetition rate 20 s^{-1}), where the arrival times were evaluated as the time difference between the trigger signal of a laser pulse and the detection time of a corresponding counted particle. The background count rate R_b on the MCP from CH^+ collisions with residual gas molecules was recorded in the breaks between the synchronized gates. The wave numbers were cycled and stayed ~4 s at each $\bar{\nu}$. The cycle included a further wave number $\bar{\nu}_{b'}$ below the $J = 3$ threshold to probe a rate $R_{b'}$ for all backgrounds, including any laser-induced one. The resonant laser-induced rates were normalized to the measured laser pulse energy ϵ_L and to R_b (proportional to the stored ion number), yielding the normalized signals $S_i = (R_i - R_{b'})/\epsilon_L R_b$. Based on updated molecular theory [25] and on a precise study of the resonance structure for our experimental parameters [29], these normalized signals can be expressed as $S_i = C\sum_J p_J \sigma_J(\bar{\nu}_i)$ with the known cross sections $\sigma_J(\bar{\nu}_i)$ and an overall normalization C. This relation is solved for the relative rotational populations p_J [29]. With electrons absent, we also performed finely spaced scans of $\bar{\nu}$ to align the experimental peaks with the J-dependent theoretical spectra. Moreover, the spectra from laser scans at $t = 14$–28 s were fitted with a linear combination of the calculated $\sigma_J(\bar{\nu})$ to derive populations $\tilde{p}_J$ ($J \leq 3$) [29] that we consider as the initial populations at $t = 21$ s for the rotational levels in the $X^1\Sigma^+, v = 0$ ground state.

As shown by the symbols in Fig. 2, relaxation by radiative transitions alone was probed for ten windows of t up to radiative equilibrium. The deduced $p_J(t)$ were fitted by the corresponding t-window averages of p_J from rate equations which included spontaneous radiative decay as well as the transitions induced by a modeled blackbody radiation field of the CSR. In this radiative model [29], the spectral intensity is composed of a cryogenic component at a temperature T_{low} with a $1 - \epsilon$ fraction of the Planck blackbody spectrum plus a small fraction ϵ of a room-temperature (300 K) blackbody spectrum from radiation leaks into CSR. With the fitted parameters $T_{low} = 14.6(21)$ K and $\epsilon = 1.03(28) \times 10^{-2}$, the radiative model

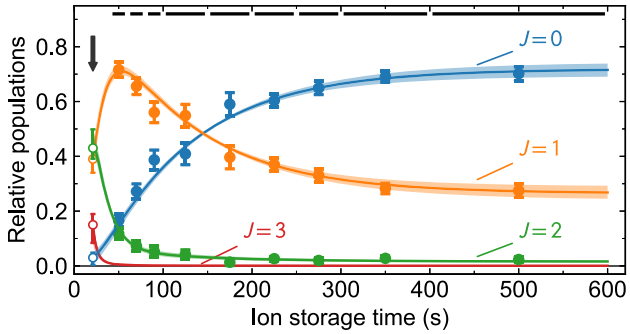

FIG. 2. Measured and modeled CH^+ rotational populations without electron interaction. Data p_J at $t > 40$ s (filled symbols and one-sigma uncertainties) were determined from the signals S_J at the J-specific laser-probing wavelengths ($J \leq 2$) averaged over the probing time windows indicated at the top (horizontal bars). Specialized laser scans (see the text) yielded populations $\tilde{p}_J$ (unfilled symbols) at $t = 21$ s (arrow) for $J \leq 3$. With these as initial conditions, the radiative model was fitted to the later p_0 and p_2 (p_1 follows as $1 - p_0 - p_2$) varying T_{low} and ϵ. Light colored bands: one-sigma uncertainties of the fitted model populations (including the $\tilde{p}_J$ uncertainties).

well reproduces the measured $p_J(t)$ and is used to predict the J populations in the stored CH^+ ions when collisional cooling by the electrons is absent. Based on the *in situ* monitoring, the remaining small population in the metastable $a^3\Pi$ state is neglected. Assuming a purely thermal radiation field, its effective temperature T_r^{eff} can be derived directly from the asymptote of the population ratio between the $J = 0$ and 1 levels, $(p_1/p_0)_{eq} = 0.39(5)$, which yields $T_r^{eff} = 19.6(11)$ K.

The effect of low-energy electron collisions was then measured (Fig. 3) by merging the velocity-matched electron beam with the CH^+ ions. Phases with electrons on and off were alternated, with the electron-off phases serving as laser-probing time windows. This results in a duty cycle for the inelastic electron interaction of ~50%. The MCP detector was activated for the laser-probing only and turned off when the electrons were on, as the high DR event rate would saturate the MCP detector.

Compared with electrons off, the $J = 0$ level now becomes populated much faster. At only 30 s of storage, $p_0 \approx 0.3$ versus $p_0 < 0.1$ without electrons. Moreover, the asymptote of the $J = 1$ and 0 population ratio, representing the equilibrium between rotational cooling and excitation, rises significantly to $(p_1/p_0)_{eq} = 0.53(13)$. Both observations reveal a strong collisional effect and directly show that in the low-temperature regime the critical electron density for the CH^+ $J = 0 \rightarrow 1$ transition is similar to or lower than our ring-averaged electron density $\bar{n}_e = 2.06(21) \times 10^4$ cm^{-3}. The larger collisional value of $(p_1/p_0)_{eq}$ indicates a somewhat higher electron temperature as compared to T_r^{eff}.

With the time dependence of the results in Fig. 3, we quantitatively test the electron-collision rate coefficients.

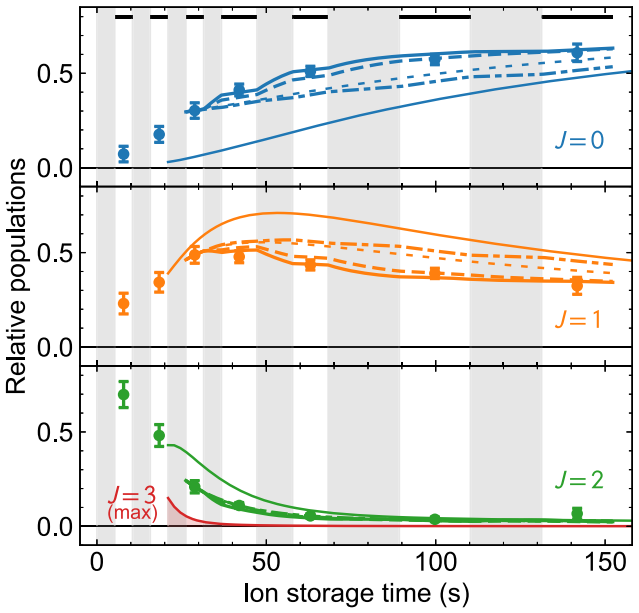

FIG. 3. Laser-probed CH^+ rotational populations p_J (symbols) with velocity-matched electrons applied in the shaded time windows. Thin full line: fitted $p_J(t)$ for radiative relaxation only from Fig. 2. The other lines show modeled evolutions starting from the $p_J(t = 28\ \mathrm{s})$ measured here. Short-dashed, radiation only; dash-dotted, depletion by J-dependent DR also included; long-dashed line, additionally including inelastic collisions using cross sections $\sigma^{\mathrm{CB}}_{J,J'}(E)$; thick full line, instead, using the R-matrix results [11] for the inelastic collisions cross sections. The red line and shaded area show the estimated maximum $J = 3$ population. Data points with one-sigma uncertainties.

We analyze the evolution of the p_J starting at $t = 28$ s, when the $J = 3$ relative population has dropped to $\lesssim 0.05$ and a three-level model ($J \leq 2$) is adequate. Even disregarding inelastic collisions, already DR as a potentially J-dependent reactive process can influence the p_J. Therefore, in addition to the radiative rates, we must account for the variation of the p_J due to differences between the DR rate coefficients for the lowest J levels. These were obtained in a separate run within the same experiment, measuring the time dependence of the merged-beams J-averaged DR rate coefficient $\bar{\alpha}^{\mathrm{mb}}_{\mathrm{DR}}(t)$ in the velocity-matched beams over 100 s of storage. These measurements required the electron energy to be rapidly alternated from a velocity-matching condition to higher values (0.2–4 eV collision energy). This led to modified $p_J(t)$ values that, during the times of detuned electron velocity, were again laser monitored. Correlating the changes of these $p_J(t)$ with those of $\bar{\alpha}^{\mathrm{mb}}_{\mathrm{DR}}(t)$, differences between the J-specific DR rate coefficients could be derived [29]. The $p_J(t)$ modeled with radiative transitions plus J-selective depletion by DR, but still excluding inelastic collisions, are separately shown in Fig. 3.

To include the inelastic collisions, cross sections $\sigma_{J,J'}(E)$ as functions of the collision energy E are used [29] to determine merged-beams inelastic rate coefficients $\alpha^{\mathrm{mb}}_{J,J'}$, thus adding the related $J \to J'$ transitions to the rate equations for $p_J(t)$. We perform this step for $\sigma_{J,J'}(E)$ calculated in the CB approximation [4,5,7,29] as well as from the most recent R-matrix calculations [11]. The latter are generally higher than the CB results by a factor of $\sim$1.6. The collision energy distribution used in the determination of $\alpha^{\mathrm{mb}}_{J,J'}$ is modeled for a set of electron temperatures $k_B T_\perp$ between 1.5 and 3.0 meV [29]. The modeled equilibrium population ratio $(p_1/p_0)_{\mathrm{eq}}$, largely governed by $\alpha^{\mathrm{mb}}_{1,0}/\alpha^{\mathrm{mb}}_{0,1}$, depends significantly on $k_B T_\perp$, but only weakly on the theoretical cross-section size. This size effectively cancels in the ratio $\alpha^{\mathrm{mb}}_{1,0}/\alpha^{\mathrm{mb}}_{0,1}$ as the cooling and excitation cross sections are related through detailed balance. Comparing Ref. [29], the model with the measured p_J at $t = 142$ s supports the experimental value of $k_B T_\perp = 2.25(25)$ meV [$T_\perp = 26(3)$ K].

The data measured at intermediate times for $p_0(t)$ and $p_1(t)$ can then be compared with the model calculations employing the experimental $T_\perp$. This probes the absolute values of the inelastic rate coefficients, dominantly $\alpha^{\mathrm{mb}}_{1,0}$ and $\alpha^{\mathrm{mb}}_{0,1}$. As seen in Fig. 3 the data are remarkably well reproduced when using the R-matrix cross sections; slightly worse agreement is found for the CB approximation.

Comparison with theory is also possible considering the thermal rate coefficients implied by the experiment. For the relevant collision energies, the J-changing cross sections for an energy level pair spaced by $\Delta E_{J,J'}$ are well approximated by a simplified, single-parameter expression. For excitation ($J' > J$), the approximation is $\hat{\sigma}_{J,J'}(E) = \hat{\sigma}^0_{J,J'} \Delta E_{J,J'}/E$ (where $E > \Delta E_{J,J'}$) with the threshold value $\hat{\sigma}^0_{J,J'}$ as the only parameter. For de-excitation, detailed balance then yields, at all energies, $\hat{\sigma}_{J',J}(E) = \hat{g}\hat{\sigma}^0_{J,J'} \Delta E_{J,J'}/E$ with $\hat{g} = (2J+1)/(2J'+1)$. An experimental value for $\hat{\sigma}^0_{0,1}$ can be obtained from the time dependence of the ratio p_1/p_0 starting at $t = 28$ s [Fig. 4(a)]. A fit of the parameter in the simplified model yields $\hat{\sigma}^0_{0,1} = 1.07(23)_{\mathrm{fit}}(40)_{\mathrm{syst}} \times 10^4$ Å^2, where the first uncertainty stems from the fitting and the second one from the uncertainties in $T_\perp$, the initial condition at $t = 28$ s, and $\bar{n}_e$. (Simplified $\hat{\sigma}_{J,J+1}(E)$ and $\hat{\sigma}_{J+1,J}(E)$ for other level pairs were included in the model with their $\hat{\sigma}^0_{J,J+1}$ matching Ref. [11], but reducing them to 0 changed the fit result by only $< 0.02 \times 10^4$ Å^2.) The simplified cross sections with the experimental $\hat{\sigma}^0_{0,1}$ and the thermal electron energy distribution at a kinetic temperature T served to obtain the plasma rate coefficients $\alpha_{1,0}(T)$ and $\alpha_{0,1}(T)$, shown in Fig. 4(b). The corresponding R-matrix results [11] and the CB approximation lie well within the experimental one-sigma uncertainty range of $\pm 43\%$.

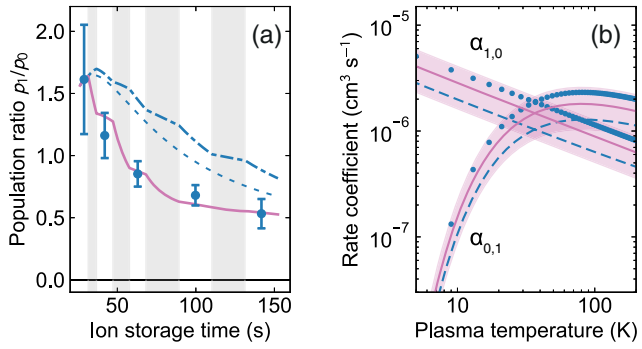

FIG. 4. (a) Population ratios p_1/p_0 corresponding to Fig. 3 (electrons applied in shaded time windows) with modeled evolutions starting from the measured populations at $t = 28$ s. Short-dashed, radiation only; dash-dotted, depletion by J-dependent DR also included; full line, additionally including inelastic collisions with the simplified $\hat{\sigma}_{J,J'}(E)$ and fitting for $\hat{\sigma}^0_{0,1}$. (b) Plasma rate coefficients $\alpha_{1,0}(T)$ and $\alpha_{0,1}(T)$ as constrained by the fitted $\hat{\sigma}^0_{0,1}$ (full lines and shaded one-sigma uncertainty), compared with R-matrix theory [11] (coalescing dots) and with the CB calculation (dashed line).

This demonstrates the use of a merged-beams electron target in a cryogenic storage ring for quantitative probing of J-changing electron collisions between the lowest rotational levels in small molecular ions. The experimental method for rotational state probing used here, employing J-dependent resonances in single-step photodissociation, generally cannot be transferred to other ion species. However, effort is underway [51] to develop J-dependent photodissociation schemes for additional small ions in cryogenic storage rings. For most systems, such schemes will include intermediate laser excitation steps similar to the resonant multiphoton dissociation process earlier realized in ion traps [52]. It will then be possible to extend the measurements to other systems crucial for spectroscopic probing of the interstellar medium, such as HCO^+. The CSR merged-beams setup offers more options for controlling and probing the electron collisions, beyond what has been realized in the present survey. Thus, future experiments may focus on precisely probing the change of p_J in a given electron interaction period or apply detuned average velocities of the electron and ion beam. This will allow electron impact excitation and de-excitation cross sections of molecular cations to be investigated in more detail, over a wider range of electron collision energies relevant not only for astrophysical environments, but also for molecular plasma conditions in general.

Financial support by the Max Planck Society is acknowledged. A. K. and D. W. S. were supported in part by the U.S. National Science Foundation Division of Astronomical Sciences Astronomy and Astrophysics Grants program under AST-1907188. We thank C. J. Williams for the NIST close coupling code used in the resonant photodissociation calculations and A. Faure for supplying the R-matrix cross sections underlying the rate coefficients published in Ref. [11].

*abel.kalosi@mpi-hd.mpg.de
†Present address: ASML Nederland B.V., Veldhoven 5504, Netherlands.
‡Present address: GSI Helmholtz Centre for Heavy Ion Research, 64291 Darmstadt.

[1] K. Bartschat and M. J. Kushner, Electron collisions with atoms, ions, molecules, and surfaces: Fundamental science empowering advances in technology, Proc. Natl. Acad. Sci. U.S.A. **113**, 7026 (2016).
[2] K. Bartschat, Electron collisions-experiment, theory, and applications, J. Phys. B **51**, 132001 (2018).
[3] M.-L. Dubernet *et al.*, BASECOL2012: A collisional database repository and web service within the Virtual Atomic and Molecular Data Centre (VAMDC), Astron. Astrophys. **553**, A50 (2013).
[4] R. F. Boĭkova and V. D. Ob''edkov, Rotational and vibrational excitation of molecular ions by electrons, Zh. Eksp. Teor. Fiz. **54**, 1439 (1968) [Sov. Phys. JETP **27**, 772 (1968)], http://jetp.ras.ru/cgi-bin/e/index/e/27/5/p772?a=list.
[5] S.-I. Chu and A. Dalgarno, Rotational excitation of CH^+ by electron impact, Phys. Rev. A **10**, 788 (1974); **12**, 725 (1975).
[6] S. S. Bhattacharyya, B. Bhattacharyya, and M. V. Narayan, Rotational excitation of molecular ions by electron impact under interstellar conditions, Astrophys. J. **247**, 936 (1981).
[7] D. A. Neufeld and A. Dalgarno, Electron-impact excitation of molecular ions, Phys. Rev. A **40**, 633 (1989).
[8] I. Rabadán, B. K. Sarpal, and J. Tennyson, Calculated rotational and vibrational excitation rates for electron–HeH^+ collisions, Mon. Not. R. Astron. Soc. **299**, 171 (1998).
[9] A. J. Lim, I. Rabadán, and J. Tennyson, Electron-impact rotational excitation of CH^+, Mon. Not. R. Astron. Soc. **306**, 473 (1999).
[10] A. Faure and J. Tennyson, Electron-impact rotational excitation of linear molecular ions, Mon. Not. R. Astron. Soc. **325**, 443 (2001).
[11] J. R. Hamilton, A. Faure, and J. Tennyson, Electron-impact excitation of diatomic hydride cations—I. HeH^+, CH^+, ArH^+, Mon. Not. R. Astron. Soc. **455**, 3281 (2016).
[12] K. Chakrabarti, A. Dora, R. Ghosh, B. S. Choudhury, and J. Tennyson, R-matrix study of electron impact excitation and dissociation of CH^+ ions, J. Phys. B **50**, 175202 (2017).
[13] A. Faure, P. Halvick, T. Stoecklin, P. Honvault, M. D. Epée Epée, J. Z. Mezei, O. Motapon, I. F. Schneider, J. Tennyson, O. Roncero, N. Bulut, and A. Zanchet, State-to-state chemistry and rotational excitation of CH^+ in photon-dominated regions, Mon. Not. R. Astron. Soc. **469**, 612 (2017).
[14] J. R. Hamilton, A. Faure, and J. Tennyson, Electron-impact excitation of diatomic hydride cations II: OH^+ and SH^+, Mon. Not. R. Astron. Soc. **476**, 2931 (2018).

[15] B. Cooper, M. Tudorovskaya, S. Mohr, A. O'Hare, M. Hanicinec, A. Dzarasova, J. Gorfinkiel, J. Benda, Z. Mašín, A. Al-Refaie, P. Knowles, and J. Tennyson, Quantemol electron collisions (QEC): An enhanced expert system for performing electron molecule collision calculations using the R-matrix method, Atoms **7**, 97 (2019).

[16] A. S. Dickinson and D. R. Flower, Electron collisional excitation of interstellar molecular ions, Mon. Not. R. Astron. Soc. **196**, 297 (1981).

[17] D. R. Flower, Rotational excitation of HCO^+ by H_2, Mon. Not. R. Astron. Soc. **305**, 651 (1999).

[18] H. S. Liszt, Rotational excitation of simple polar molecules by H_2 and electrons in diffuse clouds, Astron. Astrophys. **538**, A27 (2012).

[19] J. H. Black, Molecules in harsh environments, Faraday Disc. **109**, 257 (1998).

[20] S. Petrie and D. K. Bohme, Ions in space, Mass Spectrom. Rev. **26**, 258 (2007).

[21] B. A. McGuire, 2018 census of interstellar, circumstellar, extragalactic, protoplanetary disk, and exoplanetary molecules, Astrophys. J. Suppl. Ser. **239**, 17 (2018).

[22] D. Shafir, S. Novotny, H. Buhr, S. Altevogt, A. Faure, M. Grieser, A. G. Harvey, O. Heber, J. Hoffmann, H. Kreckel, L. Lammich, I. Nevo, H. B. Pedersen, H. Rubinstein, I. F. Schneider, D. Schwalm, J. Tennyson, A. Wolf, and D. Zajfman, Rotational Cooling of HD^+ Molecular Ions by Superelastic Collisions with Electrons, Phys. Rev. Lett. **102**, 223202 (2009).

[23] H. T. Schmidt, Electrostatic storage rings for atomic and molecular physics, Phys. Scr. T **166**, 014063 (2015).

[24] R. von Hahn *et al.*, The cryogenic storage ring CSR, Rev. Sci. Instrum. **87**, 063115 (2016).

[25] A. P. O'Connor *et al.*, Photodissociation of an Internally Cold Beam of CH^+ Ions in a Cryogenic Storage Ring, Phys. Rev. Lett. **116**, 113002 (2016).

[26] C. Meyer *et al.*, Radiative Rotational Lifetimes and State-Resolved Relative Detachment Cross Sections from Photodetachment Thermometry of Molecular Anions in a Cryogenic Storage Ring, Phys. Rev. Lett. **119**, 023202 (2017).

[27] H. T. Schmidt, G. Eklund, K. C. Chartkunchand, E. K. Anderson, M. Kamińska, N. de Ruette, R. D. Thomas, M. K. Kristiansson, M. Gatchell, P. Reinhed, S. Rosén, A. Simonsson, A. Källberg, P. Löfgren, S. Mannervik, H. Zettergren, and H. Cederquist, Rotationally Cold OH^- Ions in the Cryogenic Electrostatic Ion-Beam Storage Ring DESIREE, Phys. Rev. Lett. **119**, 073001 (2017); **121**, 079901(E) (2018).

[28] O. Novotný *et al.*, Quantum-state-selective electron recombination studies suggest enhanced abundance of primordial HeH^+, Science **365**, 676 (2019).

[29] See Supplemental Material at http://link.aps.org/supplemental/10.1103/PhysRevLett.128.183402 for the molecular parameters of CH^+, the experimental method, and the modelling of the inelastic rates, which contains Refs. [30–49].

[30] U. Hechtfischer, C. J. Williams, M. Lange, J. Linkemann, D. Schwalm, R. Wester, A. Wolf, and D. Zajfman, Photodissociation spectroscopy of stored CH^+ ions: Detection, assignment, and close-coupled modeling of near-threshold Feshbach resonances, J. Chem. Phys. **117**, 8754 (2002).

[31] P. F. Bernath, *Spectra of Atoms and Molecules*, 2nd ed. (Oxford University Press, New York, 2005).

[32] R. Hakalla, R. Kępa, W. Szajna, and M. Zachwieja, New analysis of the Douglas-Herzberg system ($A^1\Pi - X^1\Sigma^+$) in the CH^+ ion radical, Eur. Phys. J. D **38**, 481 (2006).

[33] U. Hechtfischer, J. Rostas, M. Lange, J. Linkemann, D. Schwalm, R. Wester, A. Wolf, and D. Zajfman, Photodissociation spectroscopy of stored CH^+ and CD^+ ions: Analysis of the $b^3\Sigma^- - a^3\Pi$ system, J. Chem. Phys. **127**, 204304 (2007).

[34] I. Kusunoki and C. Ottinger, Triplet $CH^+(CD^+)$ emission from chemiluminescent ion–molecule reaction $C^+(^4P) + H_2(D_2)$, J. Chem. Phys. **73**, 2069 (1980).

[35] J. L. Doménech, P. Jusko, S. Schlemmer, and O. Asvany, The first laboratory detection of vibration-rotation transitions of $^{12}CH^+$ and $^{13}CH^+$ and improved measurement of their rotational transition frequencies, Astrophys. J. **857**, 61 (2018).

[36] M. Cheng, J. M. Brown, P. Rosmus, R. Linguerri, N. Komiha, and E. G. Myers, Dipole moments and orientation polarizabilities of diatomic molecular ions for precision atomic mass measurement, Phys. Rev. A **75**, 012502 (2007).

[37] Z. Amitay, D. Zajfman, P. Forck, U. Hechtfischer, B. Seidel, M. Grieser, D. Habs, R. Repnow, D. Schwalm, and A. Wolf, Dissociative recombination of CH^+: Cross section and final states, Phys. Rev. A **54**, 4032 (1996).

[38] Ğ. Barinovs and M. C. van Hemert, CH^+ potential energy curves and photodissociation cross-section, Chem. Phys. Lett. **399**, 406 (2004).

[39] D. A. Orlov, U. Weigel, M. Hoppe, D. Schwalm, A. S. Jaroshevich, A. S. Terekhov, and A. Wolf, Cold electrons from cryogenic GaAs photocathodes: Energetic and angular distributions, Hyperfine Interact. **146/147**, 215 (2003).

[40] S. Pastuszka, U. Schramm, M. Grieser, C. Broude, R. Grimm, D. Habs, J. Kenntner, H.-J. Miesner, T. Schüßler, D. Schwalm, and A. Wolf, Electron cooling and recombination experiments with an adiabatically expanded electron beam, Nucl. Instrum. Methods Phys. Res., Sect. A **369**, 11 (1996).

[41] G. I. Budker and A. N. Skrinskiĭ, Electron cooling and new possibilities in elementary particle physics, Usp. Fiz. Nauk **124**, 561 (1978) [Sov. Phys. Usp. **21**, 277 (1978)].

[42] C. Krantz, H. Buhr, M. Grieser, M. Lestinsky, O. Novotný, S. Novotny, D. A. Orlov, R. Repnow, A. S. Terekhov, P. Wilhelm, and A. Wolf, Transverse electron cooling of heavy molecular ions, Phys. Rev. Accel. Beams **24**, 050101 (2021).

[43] P. A. M. van Hoof, R. J. R. Williams, K. Volk, M. Chatzikos, G. J. Ferland, M. Lykins, R. L. Porter, and Y. Wang, Accurate determination of the free–free Gaunt factor—I. Non-relativistic Gaunt factors, Mon. Not. R. Astron. Soc. **444**, 420 (2014).

[44] D. W. Hogg and D. Foreman-Mackey, Data analysis recipes: Using Markov Chain Monte Carlo, Astrophs. J. Suppl. Ser. **236**, 11 (2018).

[45] D. Foreman-Mackey, D. W. Hogg, D. Lang, and J. Goodman, emcee: The MCMC hammer, Publ. Astron. Soc. Pac. **125**, 306 (2013).

[46] Z. J. Mezei, M. D. Epée Epée, O. Motapon, and I. F. Schneider, Dissociative recombination of CH^+ molecular ion induced by very low energy electrons, Atoms **7**, 82 (2019).
[47] G. J. Vázquez, J. M. Amero, H. P. Liebermann, R. J. Buenker, and H. Lefebvre-Brion, Insight into the Rydberg states of CH, J. Chem. Phys. **126**, 164302 (2007).
[48] M. Larsson and A. E. Orel, *Dissociative Recombination of Molecular Ions* (Cambridge University Press, Cambridge, England, 2008).
[49] U. Hechtfischer, Z. Amitay, P. Forck, M. Lange, J. Linkemann, M. Schmitt, U. Schramm, D. Schwalm, R. Wester, D. Zajfman, and A. Wolf, Near-Threshold Photodissociation of Cold CH^+ in a Storage Ring, Phys. Rev. Lett. **80**, 2809 (1998).
[50] A. Kramida, Yu. Ralchenko, and J. Reader (NIST ASD Team), NIST Atomic Spectra Database (ver. 5.8). Available: https://physics.nist.gov/asd (2020), National Institute of Standards and Technology, Gaithersburg, MD..
[51] A. Znotins, F. Grussie, A. Wolf, X. Urbain, and H. Kreckel, An approach for multi-color action spectroscopy of highly excited states of H_3^+, J. Mol. Spectrosc. **378**, 111476 (2021).
[52] B. Roth, J. C. J. Koelemeij, H. Daerr, and S. Schiller, Rovibrational spectroscopy of trapped molecular hydrogen ions at millikelvin temperatures, Phys. Rev. A **74**, 040501(R) (2006).